Journal of Materials Chemistry A

Accepted Manuscript

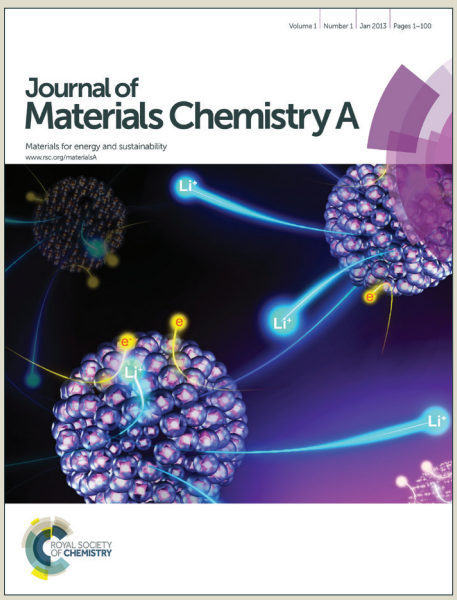

ROYAL SOCIETY OF CHEMISTRY

www.rsc.org/materialsA

Journal Name

ARTICLE

Sulfur embedded in one-dimension French fries-like hierarchical porous carbon derived from metal organic framework for high performance lithium-sulfur batteries†

Xiaofei Yang[a,b], Na Yan[a,b], Wei Zhou[a,b], Hongzhang Zhang*[a], Xianfeng Li[a,c] and Huamin Zhang*[a,c]

Received 00th January 20xx,
Accepted 00th January 20xx

DOI: 10.1039/x0xx00000x

www.rsc.org/

The lithium-sulfur (Li-S) batteries suffer from poor cycling stability caused by its own drawbacks, namely, shuttle effect, which makes it far from conquering the marketplace. To tackle this problem, a novel French fries-like hierarchical porous carbon (FLHPC) with one-dimension (1D) structure was constructed by carbonizing aluminum metal organic frame (Al-MOF). In FLHPC, sulfur was infiltrated mainly into the micro- and mesopores, while macro-pores were used to facilitate the transportation of Li ions (Li^+). On the basis of this concept, even without $LiNO_3$ as additive, the Li-S batteries not only delivered a high initial discharge capacity of nearly 1200 mA h g^{-1} at 0.1 C (1 C = 1672 mA h g^{-1}) but also showed good cycling stability of 68% capacity remained at 0.5 C after 200 cycles. In addition, when the capacity rate (C-rate) increased to 2 C, a high discharge capacity of 763 mA h g^{-1} was presented after 20 cycles, proving excellent C-rate performance.

Introduction

Rechargeable electrochemical energy storage devices with high capacity and energy density will play a more important role than ever before to meet the burgeoning development of portable electronic devices, electric vehicles and etc.[1,2] Among myriad rechargeable energy storage systems, Li-S batteries are considered as one of the most promising candidates for its superior theoretical specific capacity of 1672 mA h g^{-1} and energy density of 2600 Wh kg^{-1}, based on the low cost, environmental friendly and abundant active sulfur.[1,3,4] However, the practical application of Li-S batteries is hindered by several co-causing issues, especially low coulombic efficiency and fast capacity fading caused by the "shuttle effect" of polysulfides (PS).[3,4] To address this issue, tremendous efforts have been engaged in alleviating the diffusion of soluble PS, by wrapping with conductive host materials, such as amorphous carbon,[3,4,5-12] carbon nanotube,[13-17] carbon fibres,[18-20] graphene,[21-25] conducting polymers,[2,26] and metal oxides.[27,28]Among these host materials, the hierarchical porous carbons (HPCs) with micro-, meso- and large pores are most studied in detail[29]. It has been proved that the micro-pores in HPC could relieve the diffusion of soluble PS via strong capillary absorption. At the same time, the mesopores could help accommodate the sulfur species. Besides that, the mesopores and large pores could also facilitate the Li^+ transportation, which decreased the ohmic resistance and further improved C-rate performance of the Li-S batteries.[9]

According to the development of HPC materials, much progress of Li-S batteries has been achieved in the past decade. However, due to the insulating nature of sulfur, the high conductivity of carbon is still needed to ensure the specific capacity output.[30] The amorphous state and poor connectivity of traditional carbon powders with hierarchical porous structure often present poor electrical conductivity, thus restricting the rate performance to some extent. To overcome this problem, 1D HPC based on traditional 1D materials (eg. carbon nanotube, carbon fibre) could fabricate a conductivity network were considered as an ideal alternative.[16,20] For instance, sulfur encapsulated in the hollow carbon nanofiber@nitrogen-doped porous carbon (HCNF@NPC) core–shell composite shows excellent initial discharge capacity of 1170 mA h g^{-1} and good capacity retention of 590 mA h g^{-1} after 200 cycles at a C-rate of 0.5 C.[16] However, this kind of 1D HPCs always need somewhat inconvenient or uneconomic synthesizing procedures, which are not preferred for commercial application.[14,18] Besides that, the battery performance of 1D HPCs are also limited by low specific surface areas and low pore volumes (eg. 485.244 m^2 g^{-1} and 0.289 m^3 g^{-1} for the HCNF@NPC), which need further improvement to accommodate the volumetric expansion (~80%) from sulfur to lithium sulfide (Li_2S).[31] Hence, the 1D HPCs with relatively large specific areas, large pore volumes and proper pore

[a] Division of Energy Storage, Dalian Institute of Chemical Physics, Chinese Academy of Sciences, Zhongshan Road 457, Dalian 116023, China; E-mail: zhanghz@dicp.ac.cn; Fax:+86-411-84665057; Tel.:+86-411-84379669
[b] University of Chinese Academy of Sciences, Beijing 100039, China
[c] Collaborative Innovation Center of Chemistry for Energy Materials (iChEM), Dalian 116023 (P.R. China)

† Electronic Supplementary Information (ESI) available: [details of any supplementary information available should be included here]. See DOI: 10.1039/x0xx00000x

distribution are still needed for Li-S batteries application. In addition, more convenient and economic synthesis methods are also needed to meet the demand for factory manufacture.

Herein, a novel 1D FLHPC with a convenient synthesis method was well designed and studied for Li-S batteries application. This material was obtained by simply carbonizing Al-MOF, exhibiting large specific area and unique porous structure. As a result, excellent Li-S battery performance was successfully achieved, such as high specific capacity, good cycling stability and C-rate capability. The material preparing mechanism and the structure–performance relationship between the prepared FLHPC and Li-S batteries were studied in detail.

Experimental section

Preparation of S/FLHPC composite

The Al-MOF precursor was prepared according to A. Comotti's work.[32] Firstly, 1.500 g $Al(NO_3)_3{\cdot}9H_2O$ (Aladdin), 0.432 g 1,4-naphthalenedicarboxylate acid (1,4-H_2NDC, Aladdin) and 40 mL deionized water were placed in a 100 mL Teflon autoclave. After stirring for 0.5 h, the mixture was heated at 180 °C for 24 h to get faint yellow Al-MOF powders. Then, the Al-MOF powders were collected by suction filtration. Finally, the obtained products were washed three times with deionized water and dried under 60 °C over night.

The FLHPC was prepared according to M. Hu's work.[33]The dried Al-MOF powders were put into a ceramic boat and heated at 800 °C for 4 h, with a heating rate of 3 °C min^{-1} in a Ar filled tubular furnace. Subsequently, the samples were cooled down to room temperature in the furnace with a cooling rate of 1 °C min^{-1}. After that, 20 wt.% HF were used to remove aluminum species under magnetic stirring for 24 h. The black precipitates were then collected by centrifugation. In order to remove the aluminum species completely, the washing process was repeated 4 times. Lastly, the black precipitates were dried under vacuum conditions for 12 h at 60 °C after being further washed three times in deionized water.

The S/FLHPC composite was prepared according to previous report.[14] 0.3 g FLHPC and 0.51 g commercial sulfur (Aldrich) were dispersed into 5 mL CS_2 and stirred at room temperature until the CS_2 was completely evaporated. The obtained mixture was heated at 155 °C for 20 h under Ar atmosphere. The obtained product was named as S/FLHPC. For comparison, S/Super P composite was also synthesized under the same procedure, where super P is one of commercial carbons.

Materials Characterization

The morphology of the samples were carried out via scanning electron microscopy (SEM, JSM-7800F) using secondary electron (SE) and backscattered electron (BSE) detectors, respectively. Transmission electron microscope (TEM, JEM-2100) and Brunauer-Emmett-Teller surface area analyzer (BET, AutoSorb iQ2) were employed for pore structure studies. X-ray diffraction (XRD, DX-2700) was used for crystal structure analysis with Cu-Ka radiation (λ=0.154 nm) operated at 40 kV and 30 mA and the XRD dates were collected from 10 to 70° in 2θ at a scanning rate of 1° min^{-1}. The elements (carbon and sulfur) distribution were measured on scanning transmission electron microscope (STEM, Tecnai G2TF20) equipped with Energy Dispersive X-Ray Spectroscopy (EDX). The sulfur content of S/Super P and S/FLHPC composites were determined by using thermogravimetry analyses (TGA, Pyris-Elmer). The temperature increased from 50 to 500 °C at a heating rate of 5 °C min^{-1} under N_2 atmosphere.

Electrochemical Measurements

The electrochemical performance of the electrodes with an average active sulfur loading about 1.0 mg cm^{-2} (based on geometrical area of electrodes) was tested with CR2016 coin cells, constructed in an Ar-filled glove box. The cathodes consisted of 80 wt.% active materials (S/FLHPC, or S/Super P), 10 wt.% conductive carbon (KB600), and 10 wt.% Polyvinylidene fluoride (PVDF). These materials were first mixed with 1-methyl-2-pyrrolidinone (NMP) to form a slurry, and then casted onto Aluminium foils and dried at 60 °C for 12 hours under vacuum. Between the cathode and the anode (lithium foil) is a celgard 2325 membrane, which works as a separator. The electrolyte is 1 M bis(trifluoromethylsulfonyl) imide (LiTFSI, Aldrich) in 1, 2-dimethoxymethane (DME, Aldrich)/1, 3-dioxolane (DOL, Aldrich) (1:1 v/v) without $LiNO_3$ additive.

The cyclic voltammetry (CV) was measured with CHI 604E electrochemical workstation (Shanghai Chenhua Corp.) with a scan rate of 0.1 mV s^{-1}. The electrochemical impedance spectroscopy (EIS) measurement was conducted at open-circuit condition with a frequency range from 3.0×10^{6} Hz to 1.0×10^{-2} Hz with the amplitude of 10 mV on a Solartron 1287 electrochemical work station. The charge-discharge test was carried out using a LAND CT-2001A system at room temperature. The specific capacities mentioned in this article were expressed in mA h per gram of sulfur. The voltage mentioned in this article were respected to Li^+/Li (vs. Li^+/Li).

Results and discussion

The 1D FLHPC was prepared through one-step carbonization of Al-MOF after removing Al species with HF, as illustrated in Scheme 1. The morphology of Super P, S/Super P, Al-MOF, FLHPC and S/FLHPC was observed under SEM (Figure 1a-e). The Super P shows a particle size of nearly 30 nm and no obvious pores can be seen except some accumulated pores between particles (Figure 1a). Before sulfur impregnation, as shown in Figure 1a inset, the Super P particles exhibits good dispersion and only few particles aggregated. After sulfur impregnation, more Super P particles aggregated (the inset of Figure 1b). The morphology of obtained Al-MOF is similar to French fries (Figure 1f) with diameters less than 200 nm. Interestingly, compared to initial Al-MOF, FLHPC reserves the French fries-like morphology, but exhibits obvious large cracks or voids as a result of the carbonization and HF etching process, which is beneficial for infiltration of electrolyte during charge-discharge process. It is noteworthy that the morphology of S/FLHPC is also retained after sulfur impregnation and shows no obvious sulfur particles. Therefore, we can deduce that most of sulfur is confined

within the FLHPC.

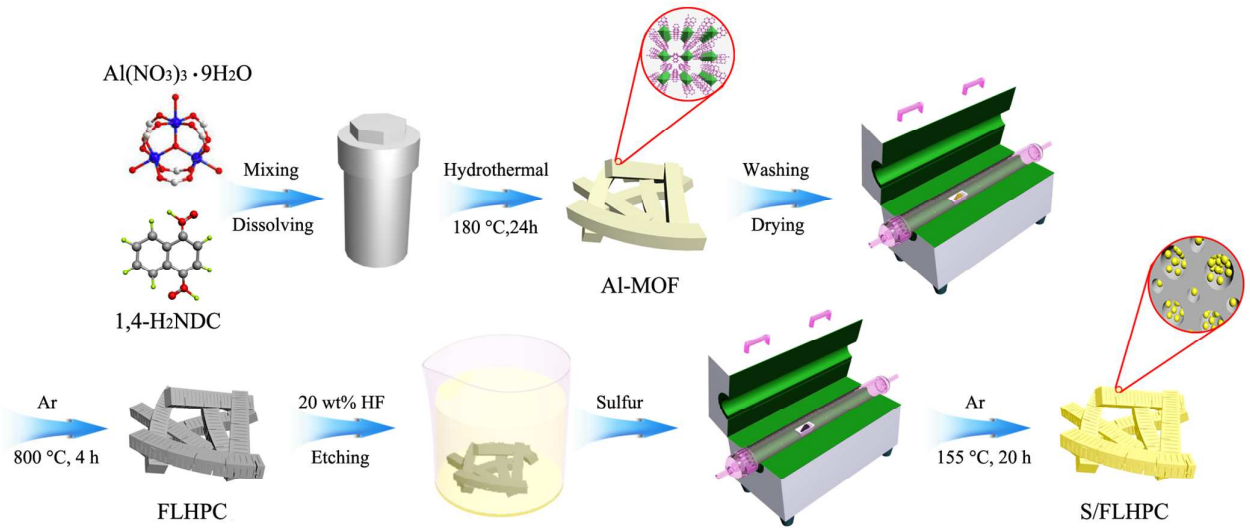

Scheme 1. Schematic illustration of the S/FLHPC composite preparation.

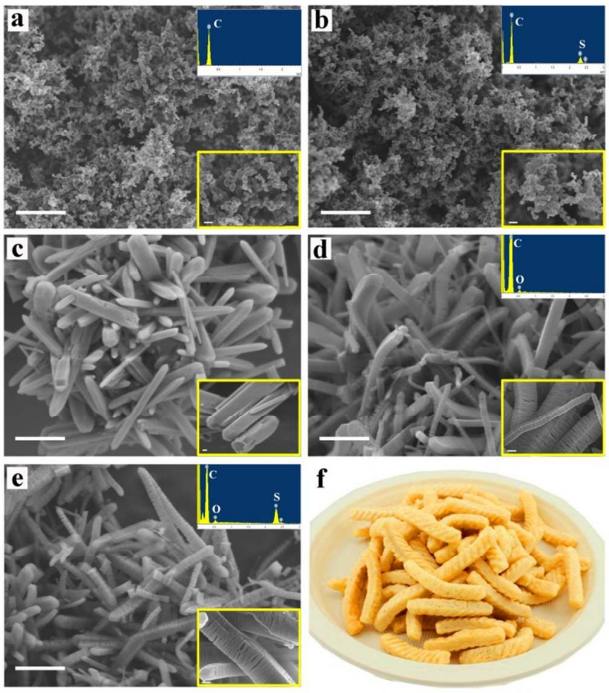

Figure 1. SEM images of: (a) Super P and (b) S/Super P with an inset at higher magnification and corresponding EDX. (c) Al-MOF with an inset at higher magnification. (d) FLHPC and (e) S/FLHPC with an inset at higher magnification and corresponding EDX. (f) French fries. The scale bars of (a), (b), (c), (d), (e)and the corresponding insets are 1 μm and 100 nm, respectively.

Furthermore, the structure of Super P, S/Super P, FLHPC and S/FLHPC in nano-scale was characterized via TEM method. As shown in Figure 2a-b, Super P with a diameter of nearly 30 nm exhibited partial graphitization and no obvious pores. After sulfur impregnation (Figure 2c-d), more Super P particles aggregated, which is coincide well with the SEM images. On the contrary, FLHPC exhibited a large amount of slit pores distributed in meso-scale (Figure 2e-f). This kind of pores owns a relatively large length/diameter (L/D) ratio, which is considered beneficial to hinder the diffusion of PS with enlonged diffusion path. It should be noticed that, after sulfur impregnation, the S/FLHPC also reserves the similar micro-structure of FLHPC (Figure 2g-h), suggesting that the sulfur is uniformally dispersed in the carbon pores. To further characterize the sulfur distribution in the host, the elemental mapping of carbon and sulfur at the selected area of STM image (Figure 2i) are shown in Figure 2 j-k, proving that the sulfur was homogenously absorbed within the FLHPC host.

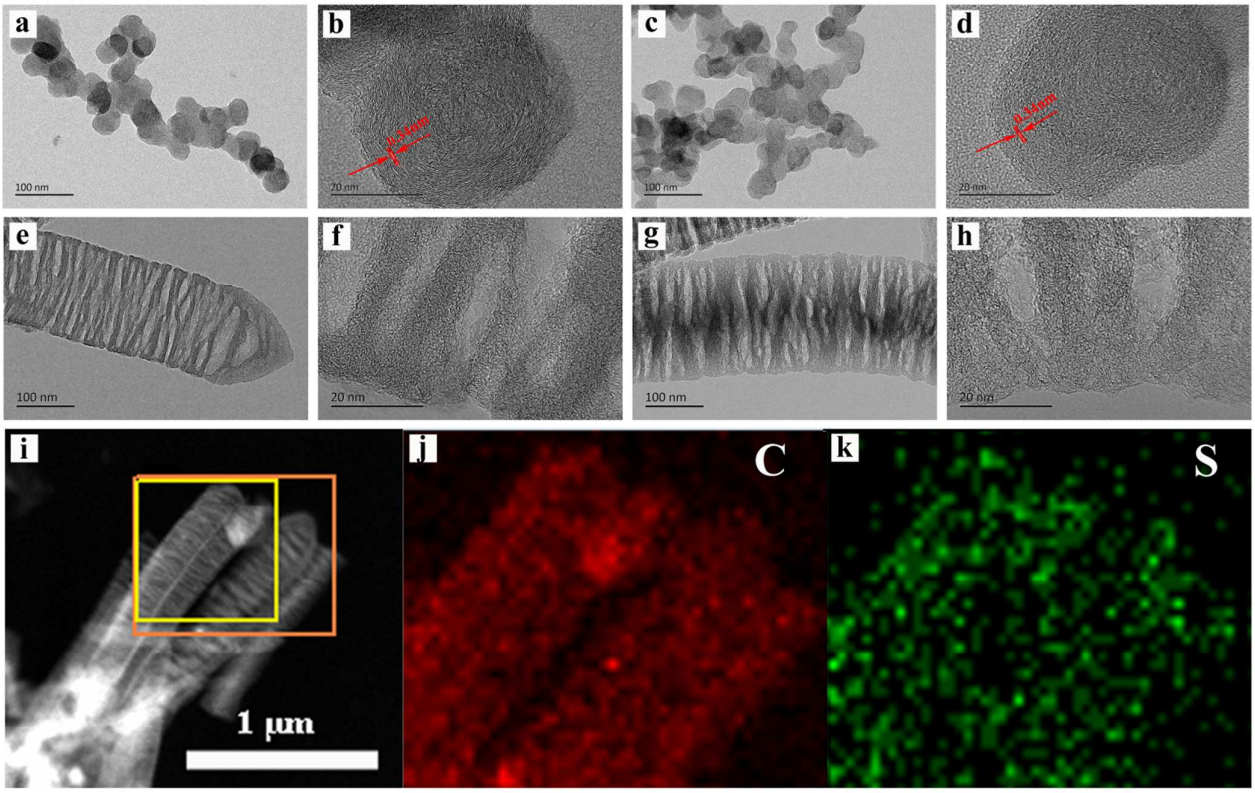

Figure 2. (a) and (b) TEM images of Super P, (c) and (d) TEM images of S/Super P. (e) and (f) TEM images of FLHPC, (g) and (h) TEM images of S/FLHPC. (i) STEM images of S/FLHPC and elemental mapping of (j) carbon and (k) sulfur.

The definite quantitative porous structures of FLHPC, S/FLHPC, Super P and S/Super P were analysed via the Brunauer-Emmett-Teller (BET) method. As shown in Figure 3a, a typical mixture of type-I and type-IV isotherm with strong absorption at low pressure and a significant hysteresis loop can be observed from the N_2 adsorption—desorption isotherm of FLHPC, indicating the existence of abundant micro- and mesopores. It can be seen from Figure 3b that FLHPC possessed two types of micropores (less than 0.5 nm and at 1.3 nm), mesopores at 5 nm and a broaden distribution from 5~25 nm on the basis of Density Functional Theory (DFT) method. According to "small molecules" theory, the pores less than 0.5 nm are beneficial to confining the sulfur as S_{2-4} and never return back to S_8, which can improve the cycling performance of Li-S batteries effectively.[13] What's more, the pores at or larger than 5 nm, which can be observed from TEM images, can also enhance the C-rate performance by facilitating Li^+ transportation. Owing to the abundant micro- and mesopores, FLHPC delivered a large surface area of 1124 $m^2 g^{-1}$ and a total pore volume of 1.00 $cm^3 g^{-1}$ (Table 1), while that of the Super P is only 57 $m^2 g^{-1}$ and 0.17 $cm^3 g^{-1}$. After sulfur impregnation, the surface area and pore volume of the obtained S/FLHPC composite decreased to 23 $m^2 g^{-1}$ and 0.15 $cm^3 g^{-1}$ respectively. Besides that, nearly all the micro- and mesopores less than 5 nm in S/FLHPC disappeared due to the sulfur impregnation. However, a part of mesopores concentrated in 8~25 nm are maintained, which could accommodate the volumetric expansion during cycles. Although the BET value of the FLHPC is not as high as the previously reported KB particles and etc, the large amount of large pores among the carbon are also much preferred according to the pervious study. [34]

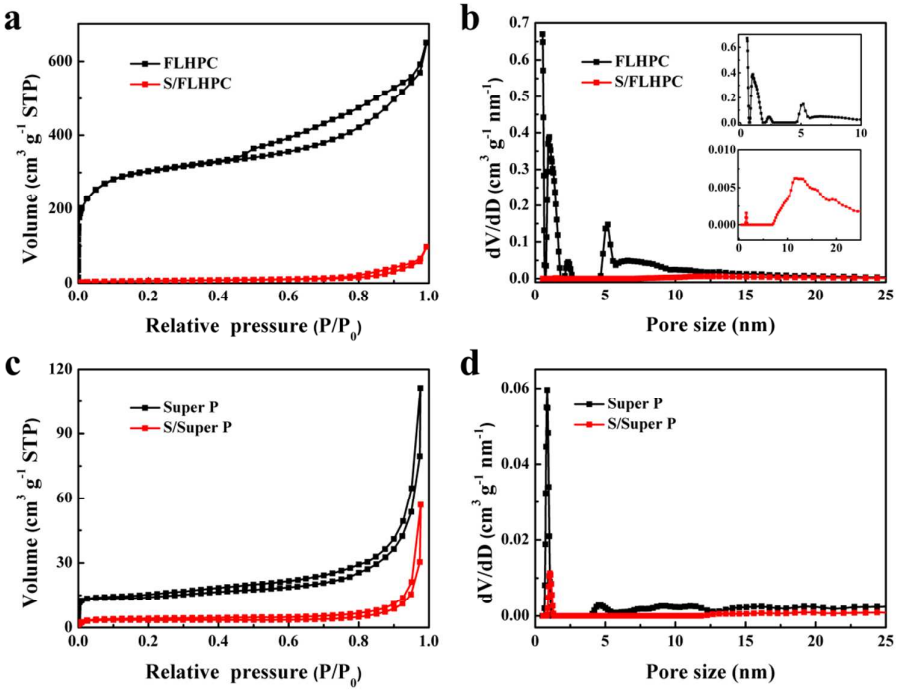

Figure 3. (a) Nitrogen adsorption—desorption isotherms and (b) pore size distribution curves of FLHPC and S/FLHPC composites. (c) Nitrogen adsorption—desorption isotherms, and (d) pore size distribution curves of Super P and S/Super P composites.

Table 1. Physical characteristics of FLHPC, S/FLHPC, Super P and S/Super P composites

Sample	BET surface area (m^2 g^{-1})	Micro-pore surface area (m^2 g^{-1})	Total pore volume (cm^3 g^{-1})	Micro-pore volume (cm^3 g^{-1})
FLHPC	1124	861	1.00	0.36
S/FLHPC	23	2	0.15	-
Super P	57	30	0.17	0.01
S/Super P	14	14	0.05	-

In order to further study the existence of the obtained S/C composite, the crystal property of the orthorhombic S, Super P, S/Super P, FLHPC and S/FLHPC are characterized via X-ray diffraction (XRD), as shown in Figure 4. For Super P, sharp diffraction peaks appeared near 26° and 44° are assigned to the (002) and (100) plane of the carbon. The peaks corresponding to crystalline sulfur with orthorhombic structure were observed from S/Super P composite, indicating that a sulfur particle size was about 76 nm as calculated with Scherrer's equation (based on (040) plane of S). On the contrary, there are no obvious peaks appeared in the XRD profile of FLHPC, suggesting comparatively low graphite degree of the porous carbon derived from Al-MOF because of a low carbonization temperature. Besides that, the peaks of crystalline sulfur are not found in S/FLHPC either, implying that most S is confined within the FLHPC pores or at least uniformally distributed in amorphous state due to a relatively large pore volume and specific surface area.

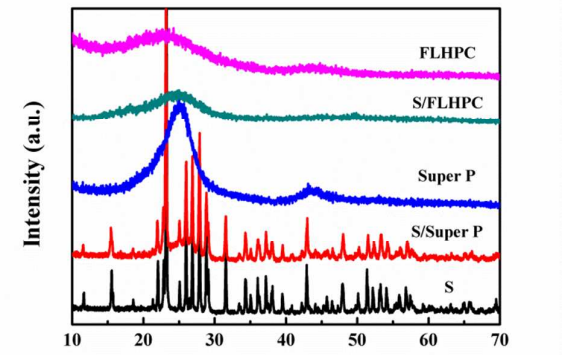

Figure 4. XRD patterns of orthorhombic S, Super P, S/Super P composites FLHPC and S/FLHPC.

The sulfur content of both S/Super P and S/FLHPC composites were characterized via TGA test. As shown in Figure 5, both composites present a weight loss of approximately 57 wt.% and 58 wt.% between 150 °C and 450 °C, which corresponds to the evaporation of sulfur in the composite materials. However, the sulfur in S/Super P quickly vanished below 280 °C, while remained at 400 °C in S/FLHPC. This output indicated that the sulfur combined

more stable with FLHPC than Super P, for a large amount of sulfur remained on the outer surface of Super P, which is in accordance with the XRD analysis. In other word, the sulfur species are more difficult to escape from the FLHPC host, which is preferred in the Li-S batteries cycling process.

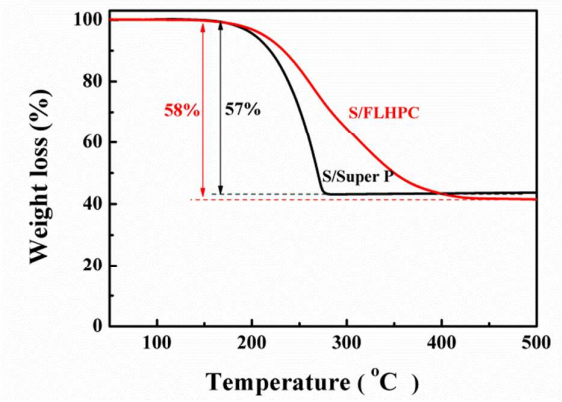

Figure 5. TGA curves of the S/Super P and S/FLHPC composites.

Figure 6a-b present the CV curves of the S/FLHPC and S/Super P composites. During negative scanning, the two peaks at about 2.3 V and 2.0 V attributed to the reduction from S to higher-order lithium PS (Li_2S_n, n≥4) and lower-order lithium PS (Li_2S_n; n<4) respectively.[35, 36] The oxidation peak at about 2.4 V exhibits the oxidation reaction of Li_2S and Li_2S_2 to final oxidation products of S. As the scanning cycles increasing, the reduction peaks' intensity of both S/FLHPC and S/Super P increase slightly, presenting an activated process. What's more, the reduction peak around 2.0 V of S/FLHPC (Figure 6a and the inset) shifted to the higher potential, meaning that the electrochemical reversibility was improved resulting from the redistribution of sulfur species [37, 38], which is similar to previous report[39]. In contrast, the corresponding reduction peak for S/Super P (Figure 6b and the inset) shifted to the lower potential, which may be resulted from the Li_2S/Li_2S_2 layer on anode caused by the uneven redistribution of sulfur and weak interactions between PS and Super P, and thus increased the charge transfer resistance of overall battery. As shown in Figure 6c, the oxidation and reduction peaks current enlarged from S/Super P to S/FLHPC electrode, which should be responses to the increase of electrochemical active sites obtained from the much higher specific surface. The electrochemical performance of both cathodes was further testified by electro-chemical impedance spectra. As shown in Figure 6d, the semicircle can reflect the resistance of the electrochemical reaction at the boundary of electrode-electrolyte, as-called charge-transfer resistance (R_{ct}). It is not hard to see that the R_{ct} for S/FLHPC electrode decreased nearly 20% compared with S/Super P (from 43 Ω cm^{-2} to 35 Ω cm^{-2}), owing to the special construction of FLHPC. On one hand, FLHPC has a large L/D ratio, so it is easy to build a conductive network to lower the resistance of electrons' transfer. On the other hand, the macro-pores derived from decomposition of organic compounds can facilitate the electrolyte infiltration and ion transfer. Last but not least, the FLHPC owns larger surface area for sulfur loading, which increased the electron transfer interface and finally led to a low R_{ct}.

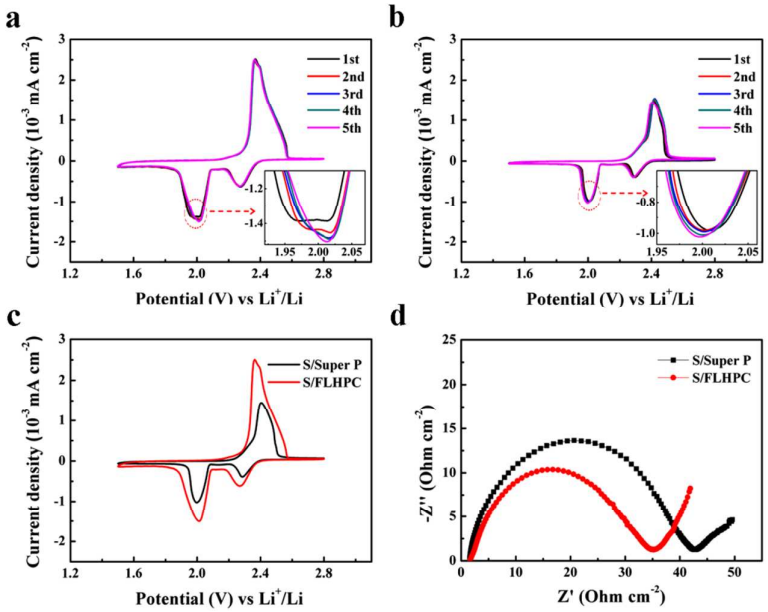

Figure 6. CV curves of a） S/FLHPC and b) S/Super P electrodes at a scanning rate of 0.1 mV s^{-1} range from 1.5 V to 2.8 V with 5 cycles; c) CV curves of S/FLHPC and S/Super P electrodes at the fifth cycle; d) EIS of S/FLHPC and S/Super P electrodes in Li-S batteries before the initial discharge.

The cycling performance of these S/C cathodes was studied at a low C-rate of 0.1 C (1 C = 1672 mA h g^{-1}) between 1.5 V and 2.8 V. As shown in Figure 7, the cell assembled with S/FLHPC cathode exhibited initial discharge capacity of 1206 mA h g^{-1}, which is much higher than the 900 mA h g^{-1} of S/Super P cathode. After 100 cycles, a high discharge capacity of 856 mA h g^{-1} (1.7 times of S/Super P electrode) was remained even in a typical electrolyte (1M LiTFSI in DME/DOL (1:1 v/v)) without $LiNO_3$ as additive, which is also better than other S/C composites derived from MOFs that have been reported.[40-43] So an excellent sulfur utilization and retention of the S/FLHPC could be concluded. Besides that, the galvanostatic charge–discharge behavior of the S/FLHPC cathode at 0.1 C during cycling was also evaluated. As shown in Figure 7b, all of discharge profiles show two obvious plateaus, meaning a two steps discharge process. Generally, the plateau around 2.3 V and 2.1 V can be ascribed to the transformation from sulfur to high-order lithium PS and further lithiation to Li_2S/Li_2S_2.[44] The much stable voltage plateaus and small capacity loss means a strong ability of FLHPC to inhibit the PS diffusion. The long-term cycling stability of S/FLHPC electrode was also tested at a rate of 0.5 C. As shown in Figure 7c, it demonstrates a high initial discharge capacity of over 1100 mA h g^{-1}. After 200 cycles, it still remained a high capacity of 751 mA h g^{-1} with a low decay rate of less than 0.16% per cycle. Such good cycling performance of S/FLHPC electrode can be mainly attributed to the relatively large specific surface, pore volume and porous distribution, which can effectively inhibit the PS diffusion.

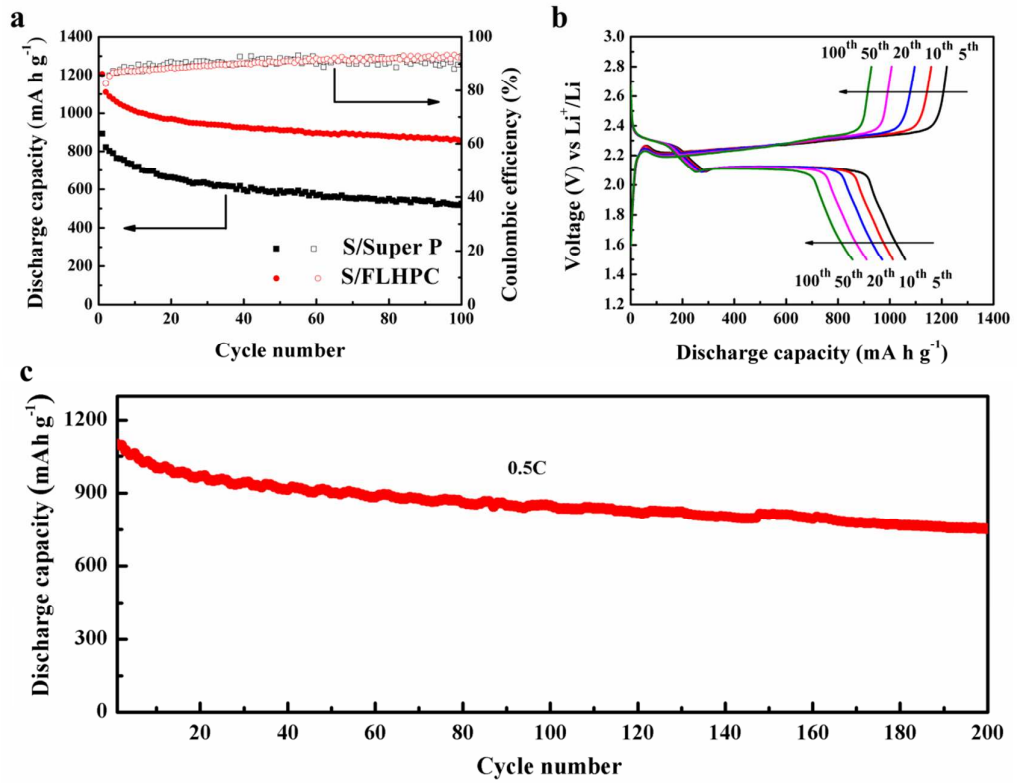

Figure 7. Electrochemical properties of the S/FLHPC and S/Super P electrodes. (a) Cycling performance of S/FLHPC and S/Super P electrodes at 0.1 C. (b) Discharge/charge curves of S/FLHPC electrode at different cycles at 0.1 C. (c) Long-term cycling performance of S/FLHPC electrode at a high rate of 0.5 C.

To further illustrate the excellent properties discussed above, an in-situ visual electrochemical experiment was conducted to study the interaction between soluble PS and the hosts, by exploiting the color change of electrolyte in an optically transparent vessel at different discharge states (illustrated and shown in Figure 8a-c). At stage a (not discharged yet), the electrolyte near S/Super P cathode and S/FLHPC cathode appeared colorless. As the Li-S batteries discharging from stage a to c, which is the turning point from the first plateau to the second one during discharge, the electrolyte with both cathodes shows gradually deepening bright brown due to the polysulfide releasing from the S/C composite. And as the Li-S batteries discharging from stage c to e, the color of both electrolytes faded obviously due to the reduction of PS to insoluble Li_2S/Li_2S_2. For comparison, the electrolyte surrounding the S/FLHPC

cathode appeared much lighter color than the S/Super P cathode from stage a to e, showing that less PS were released from the S/FLHPC composite. The visual evidence directly confirms that the FLHPC owns much stronger ability to confine polysulfide species, which could be ascribed to the well designed micro- and mesoporous structure.

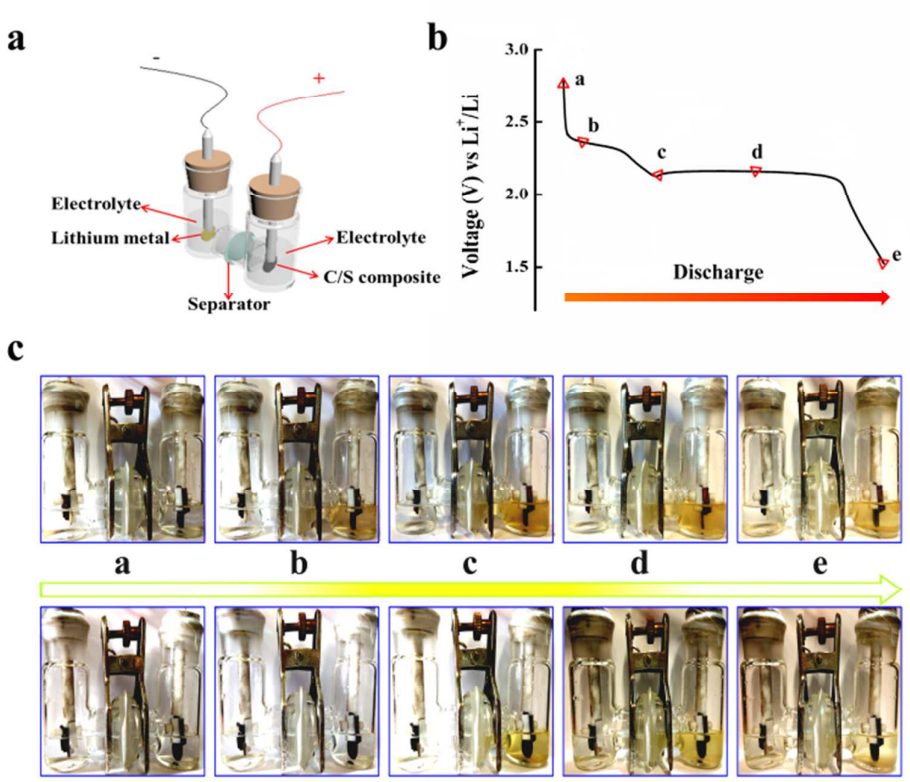

Figure 8. (a) Schematic illustration of visual–electrochemical study. (b) Schematic of a typical voltage profile. (c) Visual confirmation of polysulfide entrapment of S/Super P (up) and S/FLHPC (down) cathodes at different states of discharge from stage a to e in (b) at a C-rate of 0.05 C.

Given the unique French fries-like structure, much larger pores around micro-scale should be constructed during electrolyte preparation, which was considered important for improving the C-rate capability of Li-S batteries. The rate performances of the S/FLHPC and S/Super P cathodes were further studied and illustrated in Figure 9a. As the C-rate varied from 0.1 C to 1 C, the discharge capacity decreased gradually due to the polarization effect. However, the capacities of S/FLHPC cathodes are much higher than those of S/Super P cathodes at all current densities. For example, A reversible capacity of 763 mA h g^{-1} can still be remained at 2 C, which is much higher than the 476 mA h g^{-1} of S/Super P cathode (Figure 9b), suggesting an excellent rate capability of the S/FLHPC composites. And when the C-rate changed back to 0.1 C, the discharge capacity returned to 952 mA h g^{-1}, indicating a good stability of S/FLHPC electrode at various current densities.

In order to further understand the electrochemical performance of the cathodes, two parameters of U_1 and Q_2/Q_1 were introduced. As shown in Figure 9e, U_1 is the onset potential of the plateau at higher voltage, which can reflect the interfacial kinetics between carbon and sulfur. Q_0 represents the theoretical specific capacity of 1672 mA h g^{-1} on the basis of two electronic reaction of sulfur. Q_1 and Q_2 are the discharge capacity of the plateau around 2.3V and 2.1 V as follows:

Plateau around 2.3 V:

$$S_8 + 4e^- \longleftrightarrow 2S_4^{2-}$$

$$Q_1 = 1/4Q_0, Q_0 = 1672\ mA\,h\,g^{-1};$$

Plateau around 2.1 V:

$$2S_4^{2-} + (12 - 2n)e^- + (16 - 2n)Li^+ \longleftrightarrow nLi_2S_2 + (8- 2n)Li_2S$$

$$Q_2 = (3/4 - n/8)Q_0,\ 0 \le n \le 4,\ 1 \le Q_2/Q_1 \le 3.$$

The plateau around 2.3 V corresponds to the reduction of S to soluble PS, which amounts to 1/4 of the theory capacity due to 1/2 electron per S transferring. The plateau around 2.1 V can be attributed to the reaction of PS to final products of Li_2S, during which the insoluble Li_2S_2 and Li_2S species will generate and greatly increase the resistance of Li^+/e^- transportation. Hence, Q_2/Q_1 should

be a good indicator for reflecting the ability of Li^+/e^- transport within the host.[45] Figure 9f shows evolutions of U_1 and Q_2/Q_1 for S/FLHPC and S/Super P electrodes during the increase of C-rate. The dates were collected from charge/discharge profiles at different current densities of S/FLHPC and S/Super P as shown in Figure 9c and 9d, respectively. As can be seen, both U_1 and Q_2/Q_1 decreased gradually with the C-rate increasing, especially at high current densities due to increased ohmic polarization. Nevertheless, U_1 and Q_2/Q_1 of S/FLHPC electrodes are larger than S/Super P electrodes at all current densities, suggesting superior reaction kinetics and faster Li^+/e^- transports for S/FLHPC electrodes, which agree well with the C-rate performance. These results together highlighted the merits of FLHPC in terms of 1) the conductive network established by 1D FLHPC offers superior conductivity and 2) the interconnected hierarchical pores architecture facilitating electrolyte immersion and diffusion. Due to the improved transportation of Li^+/e^- and reaction kinetics of sulfur, the better C-rate capability of S/FLHPC could be well explained. However，when the C-rate increased to 2 C from 0.1 C, the value of Q_2/Q_1decreased seriously from 2.79 to 1.49, which might resulted from the relatively poor Li^+/e^- transport in the micro-pores at high C-rate. Hence, the next research work in our lab would be focused on further optimizing the porous distribution of the HPC derived from 1D MOFs.

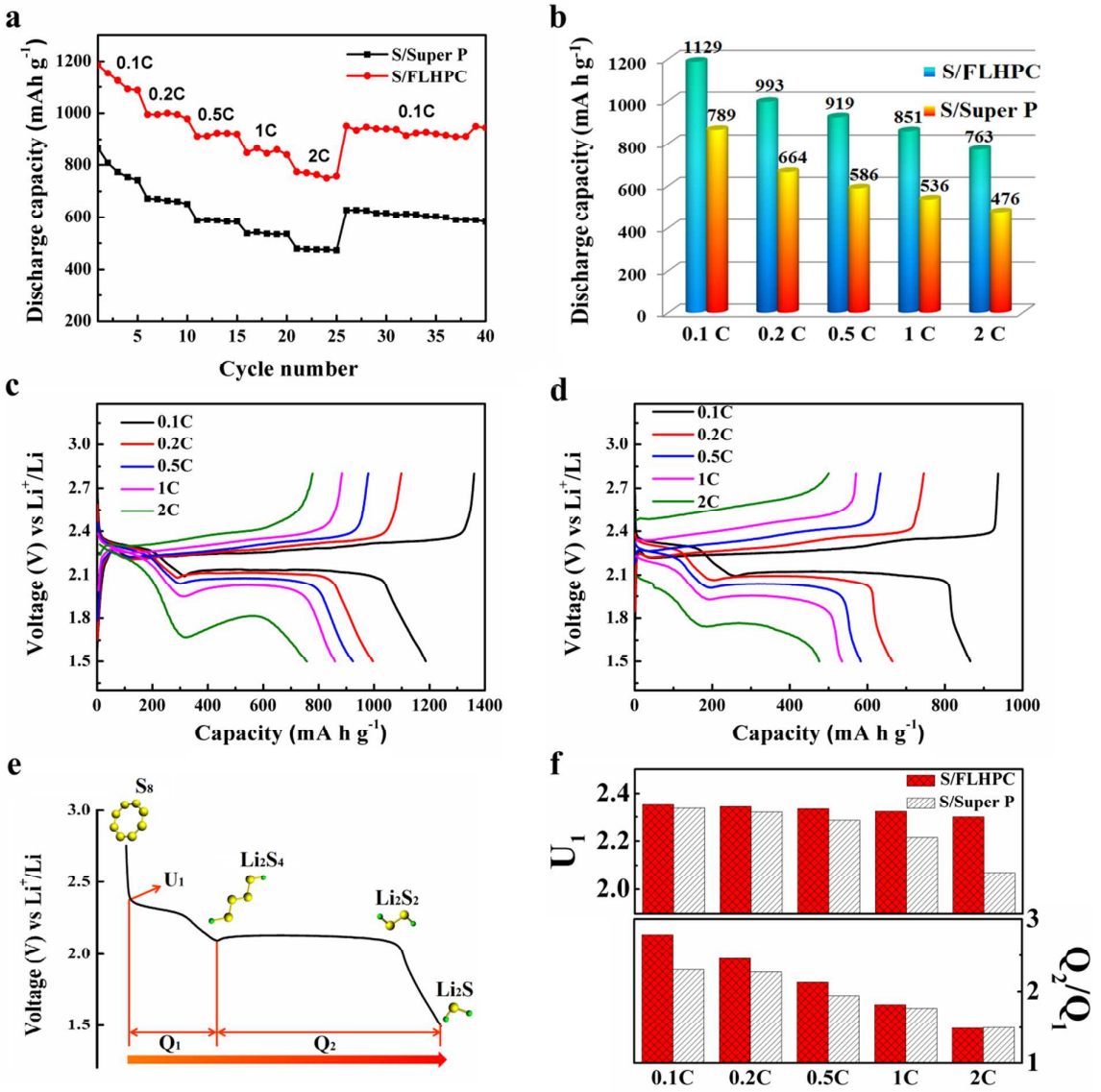

Figure 9. Electrochemical properties of the S/FLHPC and S/Super P electrodes. (a) and (b) C-rate performance for S/FLHPC and S/Super P cathodes at various C-rate from 0.1 C to 2 C. Charge/discharge profiles for (c) S/FLHPC and (d) S/Super P at various C-rate from 0.1 C to 2 C. (e) Schematic illustration of a typical voltage profile. (f) The dependence of Q_2/Q_1 and U_1 on the C- rate (data are collected from c-d).

Conclusion

In summary, we have designed a novel 1D structured French fries-like hierarchical porous carbon as an intriguing sulfur host for Li-S batteries for the first time. It could be prepared via relatively simple one-step carbonizing Al-MOF, which is promising for large scale manufacturing. Such a kind of HPC could effectively confine the PS species in the micro- and mesopores and leave enough free volume to accommodate the volume expansion from sulfur to Li_2S as well as to facilitate the Li^+/e^- transport. As a result, a high initial discharge capacity with good cycling stability as well as relatively high C-rate performance was achieved. This kind of materials might be of significant interest to the further development of Li-S batteries, and even other electrochemical devices such as capacitors and Li-O_2 batteries.

Acknowledgements

The authors acknowledge the National Natural Science Foundation of China (Grant No. 21406221 and 51403209), 100 Talents Program of Dalian Institute of Chemical Physics.

Notes and references

1 P. G. Bruce, S. A. Freunberger, L. J. Hardwick and J. M. Tarascon, *Nat. mater.*, 2012, **11**, 19-29.
2 W. Zhou, Y. Yu, H. Chen, F. J. DiSalvo and H. D. Abruña, *J. Am. Chem. Soc.*, 2013, **135**, 16736-16743.
3 J. T. Lee, Y. Zhao, S. Thieme, H. Kim, M. Oschatz, L. Borchardt, A. Magasinski, W. Cho, S. Kaskel and G. Yushin. *Adv. Mater.*, 2013, **25**, 4573–4579.
4 X. Ji, K. T. Lee and L. F. Nazar, *Nat. mater.*, 2009, **8**, 500–506.
5 S. Chen, Y. Zhai, G. Xu, Y. Jiang, D. Zhao, J. Li, L. Huang and S. Sun, *Electrochim. Acta*, 2011, **56**, 9549–9555.
6 J. Schuster, G. He, B. Mandlmeier, T. Yim, K. T. Lee, T. Bein and L. F. Nazar, *Angew. Chem. Int. Ed.*, 2012, **51**, 3591–3595.
7 J. Li, F. Qin, L. Zhang, K. Zhang, Q, Li, Y, Lai, Z, Zhang and J, Fang, *J. Mater. Chem. A*, 2014, **2**, 13916-13922.
8 G. He, X. Ji and L. F. Nazar. *Energy Environ. Sci.*, 2011, **4**, 2878–2883.
9 C. Liang, N. J. Dudney and J. Y. Howe. *Chem. Mater.*, 2009, **21**, 4724–4730.
10 B. Zhang, X. Qin, G. R. Li and X. P. Gao. *Energy Environ. Sci.*, 2010, **3**, 1531–1537.
11 N. Brun, K. Sakaushi, L. Yu, L. Giebeler, J. Eckert and M. M. Titirici, Phys. Chem. Chem. Phys., 2013, **15**, 6080–6087.
12 N. Brun, K. Sakaushi, J. Eckert and M. M. Titirici, ACS Sustainable Chem. Eng. 2014, **2**, 126–129.
13 S. Xin, L. Gu, N. Zhao, Y. Yin, L. Zhou, Y. Guo and L. Wan, *J. Am. Chem. Soc.*, 2012, **134**, 18510−18513.
14 L. Sun, M. Li, Y. Jiang, W. Kong, K. Jiang, J. Wang, and S. Fan, *Nano Lett.*, 2014, **14**, 4044−4049.
15 L. Zhu, W. Zhu, X. Cheng , J. Huang , H. Peng , S. Yang and Q. Zhang, *Carbon*, 2014,**75**, 161 –168.
16 Y. Zhao , W. Wu , J. Li , Z. Xu and L. Guan, *Adv. Mater.*, 2014, **26**, 5113–5118.
17 W. Ahn, K. Kim, K. Jung, K. Shin and C. Jin, *J. Power Sources*, 2012, **202**, 394– 399.
18 L. Ji, M. Rao, S. Aloni, L. Wang, E. J. Cairns and Y. Zhang, *Energy Environ. Sci.*, 2011, **4**, 5053–5059.
19 M. Rao, X. Geng, X. Li, S. Hu and W. Li, *J. Power Sources*, 2012, **212**, 179–185.
20 Q. Li , Z. Zhang, Z. Guo , Y. Lai , K. Zhang and J. Li, *Carbon*, 2014,**78**,1-9.
21 W. Lv, Z. Li , G. Zhou, J. Shao, D. Kong, X. Zheng, B. Li, F. Li, F. Kang and Q. Yang, *Adv. Funct. Mater.*, 2014, **24**, 3456–3463.
22 H. Li, M. Sun, T. Zhang, Y. Fang and G. Wang, *J. Mater. Chem. A*, 2014, **2**, 18345–18352.
23 G. Zhou, S. Pei, L. Li, D. Wang, S. Wang, K. Huang, L. Yin, F. Li and H. Cheng, *Adv. Mater.*, 2014, **26**, 625–631.
24 C. Xu , Y. Wu, X. Zhao, X. Wang, G. Du, J. Zhang and J. Tu, *J. Power Sources*, 2015, **275**, 22–25.
25 H. Wang, Y. Yang, Y. Liang, J. T. Robinson, Y. Li, A. Jackson, Y. Cui and H. Dai, *Nano Lett.*, 2011, **11**, 2644–2647.
26 G. Ma, Z. Wen, J. Jin, Y. Lu, X. Wu, M. Wu and C. Chen, *J. Mater. Chem. A*, 2014, **2**, 10350–10354.
27 X. Liang, C. Hart, Q. Pang, A. Garsuch, T. Weiss and L. F. Nazar, *Nat. commun.*, 2015, DOI: 10.1038 /ncomms6682.
28 Z. W. Seh, W. Li, J. J. Cha, G. Zheng, Y. Yang, M. T. McDowell, P. Hsu and Y. Cui. *Nat. commun.*, 2013, **4**, 1331-1336.
29 L. Yu , N. Brun, K. Sakaushi, J. Eckert and M. M. Titirici, Carbon ,2013, **61**, 2 4 5 –2 5 3.
30 X. Ji, and L. F. Nazar, *J. Mater. Chem.*, 2010, **20**, 9821–9826.
31 S. Moon, Y. H. Jung, W. K. Jung, D. S. Jung, J. W. Choi and D. K. Kim, *Adv. Mater.*, 2013, **25**, 6547–6553.
32 A.Comotti, S. Bracco, P. Sozzani, S. Horike, R. Matsuda, J. Chen, M. Takata, Y. Kubota and S. Kitagawa, *J. Am. Chem. Soc.*, 2008, **130**, 13664–13672.
33 M. Hu, J. Reboul, S. Furukawa, N. L. Torad, Q. Ji, P. Srinivasu, K. Ariga, S. Kitagawa and Y. Yamauchi, *J. Am. Chem. Soc.*, 2012, **134**, 2864−2867.
34 G. He, C. J. Hart, X. Liang, A. Garsuch, and L. F. Nazar, *ACS Appl. Mater. Interfaces*, 2014, **6**, 10917−10923.
35 L. Miao, W. Wang, A. Wang, K. Yuan and Y. Yang, *J. Mater. Chem. A*, 2013, **1**, 11659–11664.
36 M. Wang, Y. Zhang, H. Zhang, and H. Zhang, *ChemPlusChem*, 2014, **79**, 919 – 924.
37 Y. Su and A. Manthiram, *Chem. Commun.*, 2012, **48**, 8817–8819.
38 R. Singhal, S. Chung, A. Manthiram and V. Kalra, *J. Mater. Chem. A*, 2015, **3**, 4530–4538.
39 Z. Yang, H. Wang, X. Zhong, W. Qi, B. Wang and Q. Jiang, *RSC Adv.*, 2014, **4**, 50964–50968
40 H. B. Wu, S. Wei, L. Zhang, R. Xu, H. H. Hng and X. W. Lou, *Chem. Eur. J.*, 2013, **19**, 10804 – 10808.
41 G. Xu, B. Ding, L. Shen, P. Nie, J. Han and X. Zhang, *J. Mater. Chem. A*, 2013, **1**, 4490–4496.
42 W. Xia, B. Qiu, D. Xia and R. Zou, *Sci. Rep.*, 3: 1935 | DOI: 10.1038/srep01935.
43 K. Xi, S. Cao, X.Peng, C. Ducati, R. V. Kumar and A. K. Cheetham, *Chem. Commun.*, 2013, **49**, 2192–2194.
44 C. Tang , Q. Zhang , M. Zhao , J. Huang , X. Cheng , G. Tian , H. Peng and F. Wei, *Adv. Mater.*, 2014, **26**, 6100–6105.
45 J. Zhou, R. Li, X. Fan, Y. Chen, R. Han,W. Li, J. Zheng, B. Wang and X. Li, *Energy Environ. Sci.*, 2014, **7**, 2715–2724.

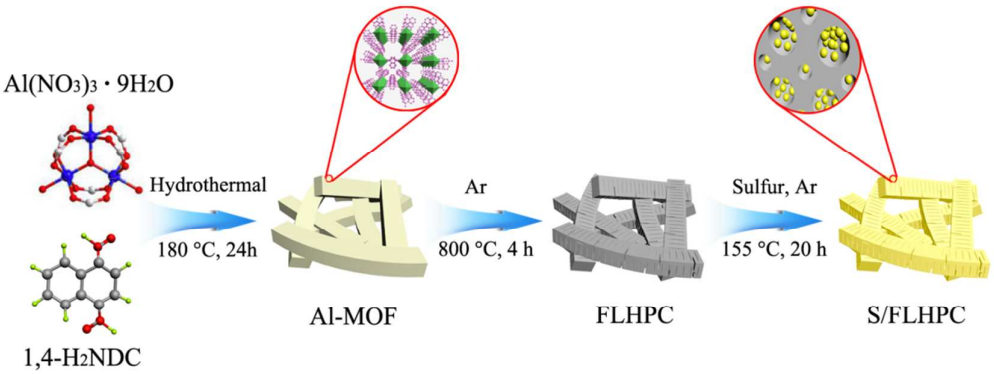

A novel one-dimension French fries-like hierarchical porous carbon with unique pore distribution was well designed for lithium-sulfur batteries.